REPORT DOCUMENTATION PAGE

Form Approved
OMB No. 0704-0188

1. REPORT DATE *(DD-MM-YYYY)*	2. REPORT TYPE	3. DATES COVERED *(From - To)*
30-08-2006	**Final Technical Report**	07-01-2005 - 05-31-2006

4. TITLE AND SUBTITLE
Basic Studies on High Pressure Air Plasmas

5a. CONTRACT NUMBER

5b. GRANT NUMBER
FA9550-05-1-0408

5c. PROGRAM ELEMENT NUMBER

6. AUTHOR(S)
Dr. Karl H. Schoenbach
830 Southampton Ave., Suite 5100

Norfolk, VA 23510

5d. PROJECT NUMBER

5e. TASK NUMBER

5f. WORK UNIT NUMBER

7. PERFORMING ORGANIZATION NAME(S) AND ADDRESS(ES)
Old Dominion University
Old Dominion University
Research Foundation
Norfolk, VA 23529

8. PERFORMING ORGANIZATION REPORT NUMBER
#253161

9. SPONSORING / MONITORING AGENCY NAME(S) AND ADDRESS(ES)

AF OFFICE OF SCIENTIFIC
875 N. Randolph,S#325,Rm 3112
ARLINGTON, VA 22203-1954
DR. ROBERT BARKER/NC
Program Manager

AF OFFICE OF SCIENTIFIC
4015 Wilson Blvd.
ARLINGTON, VA 22203-1954
JENNIFER BELL
Grants officer

10. SPONSOR/MONITOR'S ACRONYM(S)
AFOSR, AFRL

11. SPONSOR/MONITOR'S REPORT NUMBER(S)
AFRL-SR-AR-TR-06-0401

12. DISTRIBUTION / AVAILABILITY STATEMENT
Unrestricted

DISTRIBUTION STATEMENT A
Approved for Public Release
Distribution Unlimited

13. SUPPLEMENTARY NOTES

14. ABSTRACT
This project focuses on the development of diagnostic methods for electron density and gas temperature measurements of microdischarges in atmospheric pressure air, two of the most important plasma parameters for any plasma application. Two types of diagnostic techniques have being explored: emission spectroscopy for temperature measurements and two wavelength laser heterodyne interferometry for electron density. They were applied to glow discharges in atmospheric pressure air with dimensions in the millimeter range and less. Temperature measurements on this type of discharge have confirmed earlier studies where the temperature was found to be on the order of 2,000 K. A dual-wavelength heterodyne laser interferometer has been built and tested, however the results indicated, that the stability of the lasers is not sufficient for recording of the phase changes caused by these micro discharges. Suggestions for improvement of the diagnostic device are given.

15. SUBJECT TERMS

16. SECURITY CLASSIFICATION OF:			17. LIMITATION OF ABSTRACT	18. NUMBER OF PAGES	19a. NAME OF RESPONSIBLE PERSON
U					KARL H. SCHOENBACH
a. REPORT	b. ABSTRACT	c. THIS PAGE	None		19b. TELEPHONE NUMBER *(include area code)*
U	U	U			757-683-2421

Summary

The growing interest in atmospheric pressure glow discharges in air is due to a host of applications ranging from EM absorbers and reflectors to chemical and biological decontamination. The utilization of these nonthermal plasmas requires the development of plasma diagnostic techniques with appropriate spatial and temporal resolution. Parameters of interest are electron density and gas temperature. Typical values for these discharges are electron densities of up to 10^{13} cm^{-3}, and temperatures of less than 2000 K [1,2]. The goal of this project was to develop diagnostic methods, which would allow us to measure the gas temperature at an electron density of 10^{13} cm^{-3} and below with high spatial resolution (on the order of 100 μm), parameters that are relevant for a wide range of presently used atmospheric pressure air plasmas [3].

The diagnostic technique for the determination of the gas temperature is based on emission spectroscopy (rotational spectrum of the second positive system of nitrogen). An introduction to this method was presented in ref [4] by R. Block and O. Toedter. Experiments performed on atmospheric pressure discharges have confirmed earlier measurements [2]. In order to determine the electron density in atmospheric pressure air plasmas, we have developed a diagnostic system that is based on phase shift measurement using two light sources of different wavelengths. The phase shift is determined by electrons and by heavy particles. By using two wavelengths it is possible to separate the contributions of heavy particles and electrons. A CO_2 laser was provided by ODU's Applied Research Center at the Jefferson Lab, where the interferometric measurements were performed. A He-Ne laser, owned by the Center for Bioelectrics, was used as a second light source. Two-wavelength interferometry allows us to separate contributions from free electrons and neutral particle density variations that appear in atmospheric pressure glow plasmas. The dual wavelength (10.6 μm and 0.633 μm), heterodyne Mach-Zehnder interferometer was set-up and tested on an atmospheric air pressure glow discharge between pin and plate.

Experiments on this system showed that the signal–to-noise ratio of the system, particularly that of the He-Ne laser at 633 nm, was not sufficient to obtain reproducible results. Continuation of the project after termination of the AFOSR funding has been pursued with internal funds of the Center for Bioelectrics at ODU. In order to reduce the noise level, we purchased several quartz filters with a 3dB bandwidth of 3.75 kHz at 40.0 MHz. This type of filter, with a better bandwidth profile than those obtained from ONERA, are expected to allow better suppression of the noise. In addition, the purchase of a lock-in amplifier is being considered, which would allow us to considerably increase the signal-to-noise level at 633 nm.

A technical report of the project, in particular, on the electron density diagnostics, which was generated by Dr. Jerome Pons, is attached. It includes a description of the concept of the dual wavelength heterodyne interferometer, and reports the attempts to increase its sensitivity to measure phase shifts of as low as 10^{-3} degrees.

Personnel

The PI of this research project was Karl H. Schoenbach. One postdoctoral research associate, Dr. Jerome Pons, whose salary was paid by ONERA, France, joined us in April 2005 and returned to France in May of 2006. A second postdoctoral research associate, Dr. WeiDong Zhu, funded from AFOSR funds on this project, spent 50% of his time in support of the air plasma research.

Publications

Jerome Pons, Wei-Dong Zhu, Karl H. Schoenbach, and Aleksey Bugayev, "Electron Density Mapping of Atmospheric Pressure Glow Discharge in Air Using Two-Wavelength Interferometry," 2006 Intern. Conf. Plasma Science, Traverse City, MI, June 4-8, 2006, Conf. Record, paper 2P5, p. 223.
The poster for this presentation is attached.

References

[1] Robert H. Stark and Karl H. Schoenbach, "Direct Current Glow Discharges in Atmospheric Air," Appl. Phys. Lett. 74, 3770 (1999).

[2] Frank Leipold, Robert H. Stark, Ahmed El-Habachi, and Karl H. Schoenbach, "Electron Density Measurements in an Atmospheric Pressure Air Plasma by Means of IR Heterodyne Interferometry" J. Phys. D: Appl. Phys. 33, 2268 (2000).

[3] Non-Equilibrium Air Plasmas at Atmospheric Pressure, K.H. Becker, U. Kogelschatz, K.H. Schoenbach, and R.J. Barker, eds., IOP Publishing, Bristol and Philadelphia, 2005 [2] Rolf Block, Olaf Toedter, and Karl H. Schoenbach, "Gas Temperature Measurements in High Pressure Glow Discharges in Air," Proc. 30th AIAA Plasmadynamics and Lasers Conf., Norfolk, VA, July 1999, paper AIAA-99-3434.

[4] Rolf Block, Mounir Laroussi, Frank Leipold, and Karl H. Schoenbach, "Optical Diagnostics for Non-Thermal High Pressure Discharges," Proc. 14th Intern. Symp. Plasma Chemistry, Prague, Czech Republic, August 1999, Volume II, p. 945.

ONERA

Old Dominion UNIVERSITY

FINAL REPORT

Mission to Old Dominion University
(April 2005 – May 2006)

Jérôme PONS
Post-doctoral researcher (ONERA)

ACKNOWLEDGEMENTS

I wish to thank Dr. Karl H. Schoenbach for hosting me at the F. Reidy Center for Bioelectrics and for his help and support. I also thank Dr. Hani Elsayed-Ali for letting me work at the Applied Research Center and use his devices. I am grateful to Dr. Alexey Bugayev for guiding my first steps in laser optics. And of course, I'd like to give many thanks to Dr. Weidong Zhu and Nobuhiko Takano for being available anytime and helping me along with this project. Finally I'd like to thank the people from ONERA for their interest in this work and their many advises.
This work has been supported by the AFOSR.

Part I

Introduction

Aim of the mission
General matter

I.1. Introduction : summary

The mission took place at the Frank Reidy Research Center for Bioelectrics between April 1, 2005 and May 31, 2006. It has been part of a post-doctoral research project funded by the Department of Radar and Electromagnetism (DEMR) at ONERA (« Office National d'Etudes et de Recherches Aérospatiales » i.e. French Institute of Aerospace Research) which is affiliated with the French Department of Defense. The subject of this work is the space-resolved measurement of electron density in atmospheric pressure air plasmas. Plasmas with densities around 10^{13} cm^{-3} are the object of focus here.

I.2. General matter about DEMR

DEMR is one of the many departments of ONERA, and hosts about 100 people on the field of radar and electromagnetism. It is located in Palaiseau, France (20 miles SW from Paris) and Toulouse, France. The people involved in the present project are from Palaiseau, and their interest is to reduce radar cross-section of low-altitude aircrafts. Heads of the department are Jean-Louis Boulay (till September 2005) and Jean-Marc Boutry (since then). Manager of the project « Plasmas for radar cross-section reduction » is Gérard Bobillot. Other people involved are Denis Packan (plasma diagnostics), Jean-Paul Marcellin (microwaves) and Serge Larigaldie (plasma generators).
For more information about ONERA, please visit http://www.onera.fr/english.php.

I.3. Initial roadmap and final achievements

I.3.A. Initial roadmap

Hereby is summarized the roadmap for this work, as defined after two meetings at ONERA in March 2005 with the people involved in the project, who are : Dr. K. Schoenbach, J.-L. Boulay, G. Bobillot, J.-P. Marcellin, S. Larigaldie, D. Packan and J. Pons.

(a) Design and characterization of a plasma source
The first step is to design a source for the generation of a 10^{13} cm^{-3} electron density plasma in air at atmospheric pressure. The microhollow cathode stabilized glow discharge studied in K. Schoenbach's group [1] has been proposed as a source for the diagnostics, but this field has been open to other solutions.
It has been scheduled to perform experimental characterization of the plasma by electric and spectroscopic means, as well as modeling if enough time can be found.

(b) Design and setup of an electron density measurement apparatus
After listing the available diagnostic devices at CBE, 2-wavelength interferometry has been proposed as the best technique that can be setup during the time of the mission. The best for that purpose would be the use of a CO_2 laser if available, if not, other sources might be used (YAG, He-Ne...).

I.3.B. Final achievements

(a) Plasma source
The MHCD source has been studied first, but due to difficulties to build a stable, long lifetime source, other sources have been tested. The most simple, a pin-plane discharge under DC voltage,

has been finally used, and as scheduled, electrically and spectroscopically characterized. No modeling has been done due to lack of time.
An attempt to spatially extend the plasma using a linear cathode boundary layer discharge has been made at relatively low pressure (0.1 atm). However this discharge could not be run at atmospheric pressure and has been given up.

(b) N_e measurement device
A CO_2 laser and a He-Ne laser from Dr. Elsayed-Ali's group at ARC have been used, and optical and electronic components put together to set up a heterodyne Mach-Zehnder interferometer as wanted. The drawback has been the location of ARC compared to CBE (30 miles distance). Some optical elements have been borrowed from ARC, and other elements funded by the AFOSR. Lowpass filters have been borrowed from DEMR.

Devices purchased for this project are (estimate prices are given):

acousto-optic modulators with 40 MHz power supplies	$5000
- ZnSe optical components + mirrors	$1500
- infrared detector	$1000
- large recording length oscilloscope rental (1 month)	$800

The total amount is about $8000, to which must be added a 1.5 month salary to A. Bugayev for assistance in laser and optic techniques.

Part II

Technical report

Plasma-induced phase shift measurement using two-wavelength heterodyne interferometry for electron density estimation

INTRODUCTION

The aim of the present work is the experimental determination of electron density (N_e) with spatial resolution, by means of plasma-induced phase shift measurement. Two-wavelength interferometry allows in principle to separate contributions from free electrons and neutral particle density variations that appear in atmospheric pressure glow plasmas. This technique, applied for more than 30 years to fusion plasmas to compensate vibrations [4-7], has been recently proposed for micro-hollow cathode plasmas in xenon [3].

The experiment set up at ODU has consisted in testing a 10.6 μm and 0.633 μm heterodyne Mach-Zehnder interferometer before its application to an air glow plasma, in order to point out the important parameters for optimizing the instrument's sensitivity. In this part a brief theory of the interferometric method is given before detailed description of the experimentation and analysis of the results.

II.1. Theory of two-wavelength heterodyne interferometry applied to atmospheric pressure air plasma

II.1.A. Plasma-induced phase shift – Electron density determination

In this discussion a plasma with diameter 0.1-1 mm, electron density $10^{12\text{-}15}$ cm^{-3} and 2000 K rotational temperature at its center is considered. The expression of the free electron associated phase shift is reminded here :

$$\Delta\varphi_e = -r_e \lambda \int N_e(x,y)dx \quad (1)$$

r_e is the *classic radius of the electron* (2.8×10^{-15} m), λ the wavelength, x the incident beam propagation direction (a plane wave is assumed) and y the beam position (see figure 1). This expression is valid only for a wave with angular frequency $\omega >> \omega_p$ (plasma angular frequency) and $\omega >> \upsilon_c$ (dominant collision frequency in the plasma).
With the present plasma, ω_p = 10-300 GHz and $\upsilon_c \approx 10^{12}$ s^{-1} (electron-neutral collisions). Validity domain is therefore $\omega > 10^{13}$ rad×s^{-1}, or wavelengths **$\lambda < 200$ µm**.

The expression of the phase shift associated with neutral particle (gas) density variations is reminded here :

$$\Delta\varphi_g = \frac{2\pi}{\lambda}\frac{A}{N_0}\int [N_g(x,y) - N_a]dx \quad (2)$$

$A = 2.9\times10^{-4}$ (adimensional constant), $N_0 = 2.7\times10^{25}$ m^{-3} is the gas density under normal conditions (T = 273 K, p = 10^5 Pa), N_g is the gas density inside the plasma and N_a the ambient air density far from the plasma (often at 295 K and 10^5 Pa). Expression (2) is valid in air at atmospheric pressure and wavelengths **$\lambda > 500$ nm**.

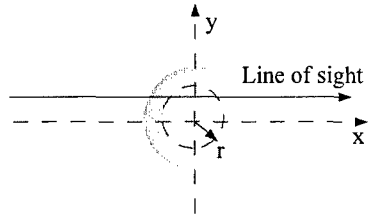

Figure 1. *Coordinates and line of sight in the plasma*

The above expressions take into account the plasma density inhomogeneity along the x-parallel line of sight at position y (figure 1). The plasma considered here has a radial symmetry with densities expressed as a function of r (for a given z plane), so that $N(x,y) = N([x^2+y^2]^{1/2})$. From the measured integral $J(y) = \int N(x,y)dx$, N(r) can be deduced using *Abel inversion* :

$$N(r) = -\frac{1}{\pi}\int_r^R \frac{dJ(y)}{dy}\frac{dy}{\sqrt{y^2-r^2}} \quad (3)$$

R is the total plasma radius, i.e. the r value such as J(y) = 0 for $r \geq R$ (NB : R is *a priori* different for electron density and gas density). The radial profile can thus be deduced from an interpolation curve J(y) determined from a series of phase shift measurements $\Delta\varphi(y_i)$. Separation of electronic and gas

phase shifts is now discussed.

Equations (1) and (2) show that $\Delta\varphi_e$ is proportional to λ whereas $\Delta\varphi_g$ is proportional to $1/\lambda$. By multiplying (1) and (2) by λ and adding both equations, the following expression is obtained :

$$\lambda\Delta\varphi = -r_e\lambda^2 J_e + CJ_g \quad (4)$$

CJ_g is independent from the wavelength (C is constant). Writing (4) at two different wavelengths λ_1 and λ_2, then subtracting the obtained expressions to each other leads to the following relation between J_e (N_e integral) and phase shifts at both wavelengths :

$$J_e = \int N_e dx = -\frac{1}{r_e}\frac{\lambda_1\Delta\varphi_1 - \lambda_2\Delta\varphi_2}{\lambda_1^2 - \lambda_2^2} \quad (5)$$

This expression reveals that the integral of N_e can be deduced from simultaneous measurements of the total phase shifts at two distinct wavelengths. The radial distribution $N_e(r)$ is then estimated from the integral. Phase shifts are usually measured using an interferometer and the method is described further.

Choosing the adequate couple of wavelengths is determined by the required precision on $N_e(r)$, i.e. the precision on J_e and the spatial resolution. The latter is determined by the plasma dimensions. The plasmas of interest here are 0.1-1 mm diameter cylindrical filaments (dimension of the ionized channel). Good spatial resolution is reached if beam diameter does not exceed 1/10 of plasma diameter. On the other hand, the minimum possible beam diameter is close to the wavelength λ. Glow discharge diameter is close to 0.1 mm. Therefore λ_1 and λ_2 should not exceed about **10 µm**. Non thermal arc has a diameter close to 1 mm, allowing wavelengths up to **100 µm**.

In the following discussion it is assumed that $\lambda_1 > \lambda_2$. If the errors on $\Delta\varphi_1$ and $\Delta\varphi_2$ are both equal to $\delta\varphi$, the uncertainty on the measured value of J_e can be expressde like:

$$\delta J_e = \frac{2}{r_e}\frac{\delta\varphi}{\lambda_1 - \lambda_2} \quad (6)$$

In order to minimize this error, both wavelengths should be as distant as possible and the uppoer wavelength λ_1 should be as high as possible (limited by required space resolution, see above). In the present work a 0.1 mm diameter glow discharge is studied, therefore $\lambda_1 \approx 10\ \mu m$ is chosen. Considering the assumptions associated with expression (1), $\lambda_2 \approx 500$ nm is an optimal choice.
It must be noted that the error on the wavelengths, i.e. their spectral width, is not taken into account in expression (6). It is easy though to check that a narrow band source minimizes the error on J_e. A frequency-stabilized laser source is an optimal choice.
Finally the error on N_e is a function of the error on J_e and the error δy on the position. The latter should be measured as accurately as possible. A manual micrometer or a remotely controlled step motor are generally used for this purpose.

The sources finally chosen and available at ODU-ARC are a CO_2 laser at λ_1**=10.59 µm**,and a laser He-Ne laser at λ_2**=632.8 nm**.

Expression (6) also shows that the absolute error on the measured phase shifts must be minimized. This point is discussed in the next section where the interferometer used for such measurements is introduced.

II.1.B. Phase shift measurement – Mach-Zehnder heterodyne interferometer

A schematic of the principle of a Mach-Zehnder interferometer is given on figure 2: a laser beam is split into two parts: one crossing the plasma and undergoing phase shift (*test beam*), the other bypassing the plasma (*reference beam*). At the end the beams are recombined. For a given value of y, the measured intensity is modulated by $\cos^2(\Delta\varphi)$, total phase shift between the beams. On a 2D detector (CCD array, photosensitive film) it leads to an interference pattern with successive dark and bright stripes. It is the most common method to visualize the phenomenon, yet it is not an accurate one (unless it is coupled with holography).

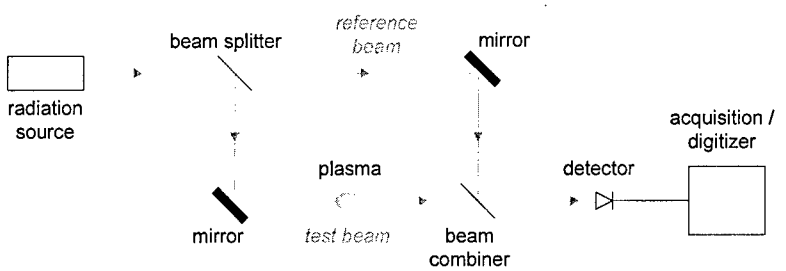

Figure 2. *Principle of a Mach-Zehnder interferometer*

A more accurate way consists in frequency-shifting the reference beam as illustrated on figure 3. With a shift of $\Delta f=\Delta\omega/2\pi$, the detected intensity after recombination varies with the frequency Δf, and **the observed signal has a $-\Delta\varphi$ phase shift**. The latter can be determined by signal processing at the output of the detector. This is the so-called heterodyne method.

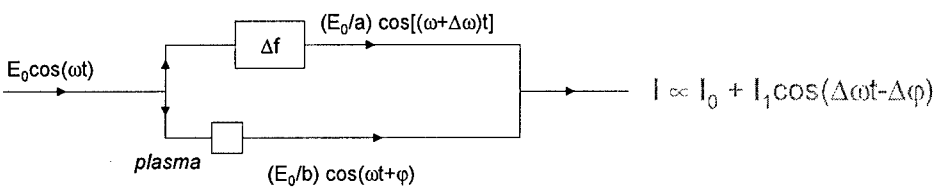

Figure 3. *Principle of a heterodyne interferometer*

NB : in principle the optical lengths are supposed equal in both branches, however an offset value of the phase shift can exist in practicle. Phase shift on the detector is the sum of plasma-induced and offset values.

As established above, the error on J_e (integral of N_e along the line of sight) is linearly dependent of the error on the phase shift. The required accuracy on $\Delta\varphi$ is thus determined by the minimum error allowed on J_e. The error on the phase shift can be interpreted in terms of signal-to-noise ratio with the following expression:

$$\left(\frac{S}{N}\right)_{dB} \geq -20\log_{10}(\delta\varphi)$$

In order to predict the minimum accuracy of the instrument, values ranges of electronic phase shifts are calculated for different possible conditions. A 0.1 mm diameter plasma probed with a 10 µm wavelength laser, and a 1 mm diameter plasma probed with a 100 µm laser are considered below. Corresponding values of phase shift and signal/noise ratios are reported in tables 1a and 1b.

N_e (cm^{-3})	10^{12}	10^{13}	10^{14}	10^{15}
$\Delta\varphi_e$ (°)	1.6×10^{-4}	1.6×10^{-3}	1.6×10^{-2}	0.16
S/N (dB)	130	110	90	70

Table 1a. *Plasma 0.1 mm, laser 10 μm*

N_e (cm^{-3})	10^{12}	10^{13}	10^{14}	10^{15}
$\Delta\varphi_e$ (°)	1.6×10^{-2}	0.16	1.6	16
S/N min (dB)	90	70	50	30

Table 1b. *Plasma 1 mm, laser 100 μm*

Minimal signal/noise ratios are calculated considering a measurement with a 10% precision, i.e. $\delta\varphi=\Delta\varphi_e/10$.

These tables give an overview of minimum signal quality to measure the phase shifts properly. It shows that the signal/noise ratio must be optimized, i.e. the signal must be maximized and the noise minimized.
On the other hand, it is important to consider drifts or fluctuations of heterodyne frequency Δf and phase shift $\Delta\varphi$. These parameters vary with a given characteristic time, and can be considered approximately stable only if data acquisition is performed during a much shorter time.

In the next chapter (II.2) the interferometer built at ARC at wavelengths 10.59 μm and 632.8 nm and heterodyne frequency 40 MHz is described. Stability and sensitivity of the instrument are estimated and discussed in chapter II.3.

II.2. Experimental setup

II.2.A. Interferometer: overview

Figure 4 shows an overview of the interferometer.

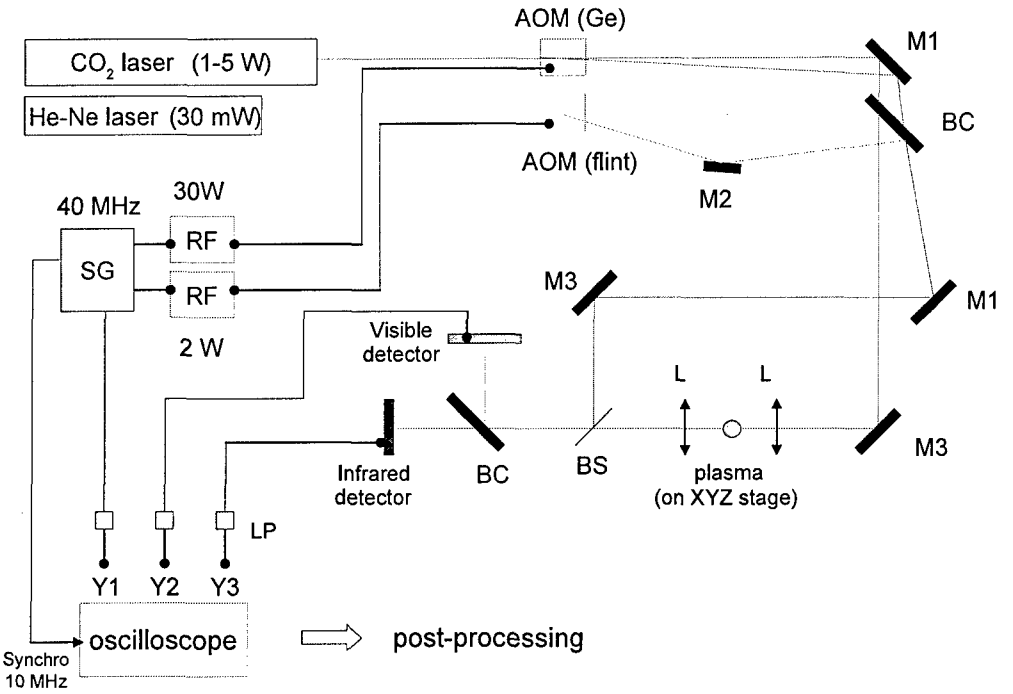

Figure 4. *Mach-Zehnder heterodyne interferometer*

Captions:

AOM: acousto-optic modulator	M1: Au mirror
BC: beam combiner	M2: Al mirror
BS: beam splitter	M3: Al/SiO_2 mirror
L: converging lens (f = 10 mm)	RF: 40 MHz RF power supply
LP: low-pass filter (cutoff 44 MHz)	SG: signal generator

A tunable CO_2 laser emitting a few watts at 10.6 μm, and a 30 mW He-Ne laser at 632.8 nm are both split in two beams, one of them is frequency-shifted of 40 MHz by means of an acousto-optic modulator. Unshifted beams are combined using a parallel plate and form the test beam, shifted beams are combined to form the reference beam. Test beam is focused on the plasma and defocused using a pair of converging lenses (plasma is at the focal point of both lenses). Once the beams recombined using a beamsplitter, both wavelengths are separated using a beamcombiner and detected individually. Signals at frequency 40 MHz are acquired using an oscilloscope and compared to the signal out of the signal generator that drives the RF power supplies. Phase shifts are calculated after post processing.
Dimensions : distance between AOM and beam splitter is about 1 m in the infrared and 2 m in the visible.

II.2.B. Detailed description of the elements in the interferometer

(a) Lasers

CO_2 laser is an Advanced Kinetics (Adkin) model MIRL-50 (company no longer exists and model is no longer manufactured). It is made of a water-cooled, discharge tube supplied by DC current (10 mA) in which runs the low pressure (1 kPa) lasing medium (13% CO_2, 22% N_2, 65% He). The tube is placed inside a cavity, made of a grating for line selection (between 9 and 11 µm) and an output mirror (partly transmitting). The laser beam is vertically polarized and mode selective (TEM_{00}). At 10.59 µm the output power is of a few watts under the above pressure and current conditions, and the beam has a diameter of a few millimeters out of the output mirror.
He-Ne laser is a Spectra Physics model 127 (no longer manufactured) emitting a 30 mW horizontally polarized beam at 632.8 nm, TEM_{00}, with a diameter close to 1 mm out of the cavity with a 0.66 mrad divergence. Photographs in figure 5 show both lasers on the optical table.

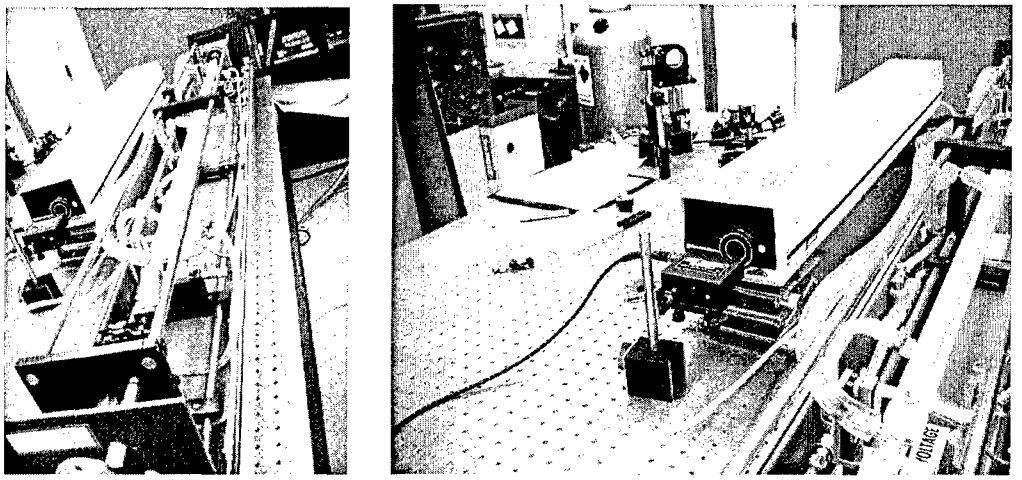

Figure 5. *Adkin MIRL50 CO_2 laser (without cover) and SP127 HeNe laser (white cover) Brewster window out of the discharge tube on the Adkin laser can be regognized, as the visible range AOM displayed beyond the SP laser*

(b) Acousto-optic modulators (AOM)
Principle
An AOM is made of solid material across which an acoustic wave propagates in a given direction at the frequency F. This wave generated periodic density variations in the material, that consequently behaves like a grating. A radiation beam crossing the AOM is thus diffracted into several orders. At a particular incidence angle (compared to the acoustic wave propagation direction) called the *Bragg angle*, only the 0^{th} and 1^{st} order beams are generated. Bragg angle θ_B is equal to the half of the deviation angle (angle θ between 1^{st} and 0^{th} order beams), and expressed as follows:

$$2\theta_B = \theta = \frac{\lambda F}{v} = \frac{n\lambda_0 F}{v}$$

λ is the beam wavelength in the material, equal to $n\lambda_0$ where n is its refractive index and λ_0 the wavelength in vacuum, and v the acoustic wave velocity in the material. Therefore Bragg angle depends on the material and the beam properties. In general the incidence angle is chosen equal to θ_B (Bragg regime). The AOM is then called a *Bragg cell* (NB : in normal incidence the AOM works in the Raman-Nath regime).
On the other hand the m^{th} order beam (m relative integer) is frequency shifted of mF compared to the incident beam, because of a Doppler-like effect. In an interferometer a Bragg cell is both a beam splitter and frequency shifter. Moreover is it possible to balance the intensities of 0^{th} and 1^{st} order beams by adjusting the acoustic power.

Characteristics

The AOMs and their 40 MHz power supplies are from IntraAction: model AGM-406B1 in the infrared with 30 W supply model GE-4030-N, and model AOM-40 in the visible with 2 W power supply model ME-402-N.

The AGM406 is made of germanium crystal, efficiently diffracting a 10.59 μm beam polarized in the acoustic wave propagation direction. Bragg angle is 38.5 mrad.

The AOM40 is made of dense glass (flint) and diffracts any beam in the range 440-700 nm with any polarization. Bragg angle is equal to 3.25 mrad.

Power supplies have their own internal quartz oscillator generating a 40 MHz signal with a 30 ppm precision, however since synchronization between both AOMs is necessary they are externally driven by a signal generator Leader model LG3226 (no longer manufactured) generating -133 to +13 dBm in the range 100 kHz to 2 GHz (5 ppm precision). NB: the better precision is also a criterium in the choice of a driver, since the error on the frequency leads to an error on the phase shift.

(c) Optical elements

Mirrors

Protected mirrors must be used to stand the high CO_2 laser flux. M1 mirrors have a gold coating and M3 mirrors have an aluminum coating protected by a silica (SiO_2) overcoating. Au reflectivity is better than Al (at 10.6 μm: Au 99%, Al 98% - at 632.8 nm: Au 97%, Al 88%). To balance losses between reference and test beams, an M3 mirror is used in each.

M2 mirror has an unprotected Al coating and is only used with He-Ne laser radiation. Its purpose is to deviate the visible 1st order beam so as to align it with the infrared one (Bragg angles are different at both wavelengths).

M3 mirrors are from Janos Technology (model A2010-282).

Beam combiners, beam splitters

A parallel plate combines or splits a beam according to its properties. However it is named beam splitter or beam combiner according to a standard definition that is also the commercial one:

- a beam combiner **combines or splits** beams with **distinct wavelengths**. Ideally, it is totally transparent to one of the wavelengths and totally reflective to the other;
- a beam splitter **combines or splits** beams with **similar wavelengths**. Ideally it is equally transmittive and reflective (R=T=50%).

Both are generally optimized for 45° angles of incidence.

Note that in figure 2, the plate called beam combiner is in fact a beam splitter according to this definition.

NB : among the beam splitters, there is a variety called « polarizing beam splitter », that ideally is 100% transparent to one polarization direction and 100% reflectant to the orthogonal direction. S-polarizing plates reject beams polarized in a direction parallel to the incidence plane, and P-polarizing plates reject beams polarized in a direction perpendicular to that plane. In the present application a non-polarizing plate must be used.

The beam splitter used here is made of zinc selenide (ZnSe), transparent to both wavelengths (NB: germanium is transparent to IR but not to visible). It is optimized for 10.6 μm in standard conditions (R/T=50/50 at 45°), but R/T is smaller at 632.8 nm. Important losses of the reference visible beam thus occur at the beam splitter, leading to a strong DC component on the detected signal.

The beam splitter is from Cradley-Crystals.

Beam combiners are made of ZnSe with coating on one face with a reflectivity of about 90% at 632.8 nm and 45°, and an optimal transmittance at 10.6 μm. Their thicknesses are 2 mm. They are

from Laser Research Optics (model BC-1008-Z-AR-U670).

Lenses

Laser beam diameter is typically about 1 mm at the cavity output with a divergence angle of a few milliradians. It is therefore necessary to focus the beam in order to reach the required spatial resolution. The focal spot diameter depends on the lens focal length. The following expression can be applied to a perfectly gaussian beam:

$$w_F = \frac{\lambda f}{\pi w_L}$$

λ is the wavelength, f the focal length and w_L the beam diameter on the lens (the beam is assumed to have a small divergence angle). Here it is assumed that w_L = 5 mm. At λ = 10 µm, if a spatial resolution of 10 µm is expected a focal length of 15 mm is required. Practically such lenses are hard to insert knowing the discharge generator dimensions (see below). In the present system f = 100 mm is used, leading to w_F = 60 µm. Spatial resolution is thus lower but it allows for an easier alignment. Plano-convex ZnSe lenses are chosen. The focal length is determined at the wavelength 10.6 µm. At 633 nm the refractive index of ZnSe is different, so is the focal length. The focal length of a lens with spherical faces is expressed as follows:

$$\frac{1}{f} = (n-1)\left(\frac{1}{R_1} - \frac{1}{R_2}\right)$$

R_1 and R_2 are the radii of each face. Ratio of focal lengths is thus expressed as:

$$\frac{f(\lambda_1)}{f(\lambda_2)} = \frac{n(\lambda_2)-1}{n(\lambda_1)-1}$$

For ZnSe $n(\lambda_1$=10.6 µm) = 2,4 and $n(\lambda_2$=0.633 µm) = 2,6, so f(0.633 µm) = 88 mm. However at 0.633 nm the focal spot diameter is about 3 µm, so that across the plasma the actual beam diameter is close to that of the CO_2 laser. The same lenses can therefore be used for both wavelengths.
A pair of ZnSe lenses with f = 100 mm from Cradley Crystals is used.

(d) Detectors

Visible detector

It is a PIN Si photodiode (ThorLabs model Det110) with an active area of 13 mm^2, sensitive to wavelengths in the range 350-1100 nm. For 50 Ω load impedance (oscilloscope input impedance), its bandwidth is 160 MHz, and at 633 nm the output voltage / input power ratio is 20 mV/mW (dark current 20 nA, corresponding to 20 µV; linearity limit 1 mW). The noise-equivalent power is 1.2×10^{-14} $W\times Hz^{-1/2}$.

Infrared detector

It is a HgCdZnTe photoelectromagnetic detector (VigoSystems PEM10.6 sold by Boston Electronics) with an active surface of 1 mm^2, sensitive in the range 2-12 µm and working at ambient temperature. Bandwidth it higher than 350 MHz, and at 10.6 µm the output voltage / input power ratio is 40 mV/W (for a 50 Ω load impedance).Normalized detectivity is 4×10^6 cm $Hz^{1/2}$ W^{-1}.

(e) Acquisition system and filters

Oscilloscope

It is a Tektronix TDS 7404 oscilloscope with a maximal sampling rate of 20 GS/s (5 GS/s per channel, 4 channels), 4 GHz bandwidth and a maximal recording length of 1 MS. Samples are digitized on 8 bits (256 levels).

Lowpass filters

They are Chebyshev filters with a cutoff frequency of 44 MHz, and come from Wainwright Instruments (model WLK44-4SS). Their use allows to reduce the acquisition bandwidth and

consecutive noise spectrum folding. The noise spectrum, assumed to be an ideal white noise, is spread on the sampling frequency bandwidth, which is set at 250 MHz under the present conditions. If the acquisition is done on a higher bandwidth, like the oscilloscope 4 GHz bandwidth, the noise is folded on a narrower bandwidth and its level is increased. If the opposite effect is wanted, it is necessary to reduce the measurement bandwidth and thus proceed to filtering. Ideally bandpass filters are most suitable to this purpose. Note that this effect is limited to the noise level in the 40 MHz line, that is determined by the detector and oscilloscope sensitivities, generally high however.

Post-processing

Processing of recorded files has been done using Matlab 7.1.

II.3. Results : analysis and discussion

II.3.A. Discharge

(a) Description and electrical properties

The plasma studied here is generated by a glow discharge in air at atmospheric pressure between a positively biased pin and a grounded plane separated by a gap of a few millimeters (see figure 6a). The discharge is maintained by a 5 kV, 40 mA DC voltage power supply (Bertan model 210-05R) across a 100 kΩ ballast resistor in series. The plasma exhibits classic characteristics of a glow discharge (positive column, cathodic spaces...) as illustrated on figure 6b.

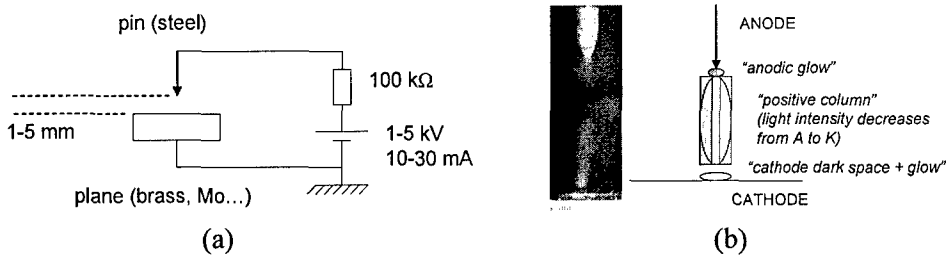

***Figure 6**. (a) Discharge setup (b) Photograph and schematic of the glow discharge structure*

The voltage-current characteristic is presented on figure 7a, for different cathode materials and a 5 mm gap. The discharge has a negative differential resistance (dU/di), i.e. voltage tends to decrease when current increases. Figure 7b shows that for a given current value voltage increases with the gap, i.e. the electric field in the discharge remains constant. Extrapolation of the line U=f(d) to a gap equal to 0 gives an estimate value of the voltage across the cathodic space of about 300 V. Note that such a discharge has been studied for more than 50 years [8] but seldom used for a potential industrial application until recently.

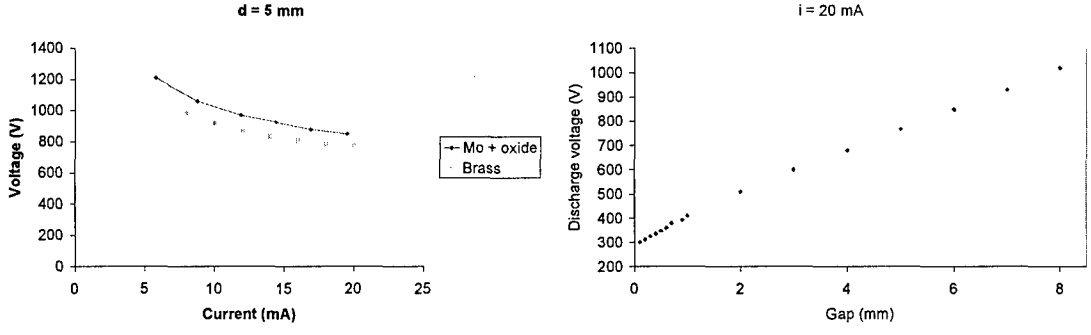

***Figure 7**. (a) Voltage vs. current, fixed gap ; (b) Voltage vs. gap, fixed current*

Non oxidizable cathode material is chosen, or entirely covered by a thin oxide layer. Staack et al [9] have noticed that non oxidizable materials let a stable cathode spot be established, whereas this spot tends to move on oxidizable material, leaving oxide behind its path. This phenomenon has been observed here using steel or aluminum, whereas brass produces a stable discharge. Surprisingly pre-oxidized molybdenum also produces a stable discharge, letting breakdown occur at a point that becomes conductor then. Breakdown leaves a crater that has been observed using a microscope after several hours of operation (see figure 8). However this crater tends to enlarge itself and cathode spot becomes more and more unstable on it. Non oxidizable material is then preferable.

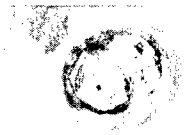

Figure 8. *Conductive crater left after breakdown on oxidized molybdenum*

Average electron density estimation

For a given current the value of plasma resistance gives an estimate average electron density. N_e is related to the conductivity γ and the resistance by the following expressions:

$$\gamma = \frac{N_e e^2}{m_e \nu_c} = \frac{d}{RS}$$

υ_c is the electron-neutral collision frequency, m_e the electron mass (9×10^{-31} kg), d the gap and S the plasma cross-section area (assuming a cylindrical geometry). For a brass cathode, a 20 mA current and a 5 mm gap R = 40 kΩ. The radius and therefore S are not known precisely, but it is reasonable to think that the radius is between 0.1 and 1 mm. The value of υ_c depends on neutral particle density and is expressed as:

$$\nu_c = N_g \sigma_c \sqrt{\frac{k_B T_e}{m_e}}$$

T_e is the electron temperature, σ_c the elastic collision cross section, k_B Boltzmann constant. In air $\sigma_c = 2.75\times10^{-19}$ m^2. k_BT_e is assumed to be close to 2 eV (vibrational energy barrier of nitrogen). At ambient temperature T_g = 293 K, $N_g = 2.5\times10^{25}$ m^{-3}, therefore $\upsilon_c = 4.1\times10^{12}$ s^{-1}. At T_g = 2000 K, $N_g = 3.6\times10^{24}$ m^{-3} and $\upsilon_c = 6.6\times10^{11}$ s^{-1}. 10^{12} s^{-1} is the range of values that is considered for this estimation (see chapter II.1, same range considered). Consecutive values of conductivity and electron density are:

r = 0.1 mm : $\gamma = 4$ Ω^{-1}m^{-1} and $\mathbf{N_e \approx 10^{14}\ cm^{-3}}$
r = 1 mm : $\gamma = 0.04$ Ω^{-1}m^{-1} and $\mathbf{N_e \approx 10^{12}\ cm^{-3}}$

The electron density is likely bounded by these extreme values and $\mathbf{10^{13}\ cm^{-3}}$ can be regarded as a mean value. From II.1 discussion, it corresponds to signal/noise ratios of around **100**.

(b) Spectral properties

Figure 9 shows part of the plasma near-UV emission spectrum for a 3 mm gap and a 20 mA current. Molecular bands can be identified: NO (γ system, 200-260 nm), OH (0-0 band, 305-320 nm) and N_2 (2nd positive system, 320-400 nm). Spectra were recorded using an Acton Research (ARC) spectrometer SpectraPro-500i with a 3600 grooves/mm grating and a photomultiplier tube.

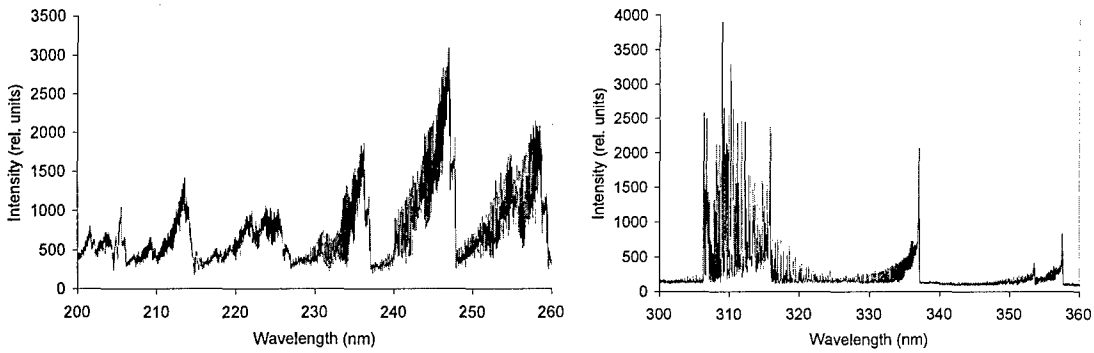

Figure 9. *Plasma UV emission spectrum*

A simulation of the OH band with the LIFBASE software (version 2.0.55) shows that rotational temperature corresponding to the above spectrum is close to 4000 K (figure 10). Note that LIFBASE assumes local thermodynamic equilibrium.

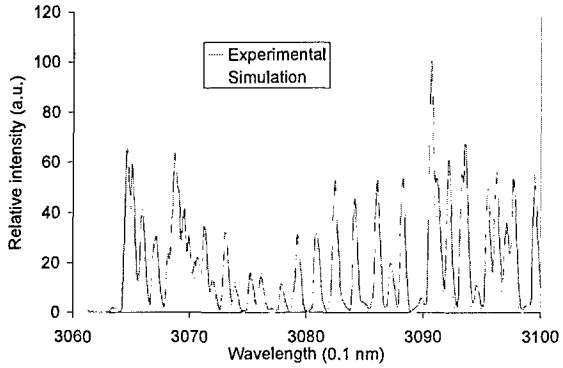

Figure 10. *OH experimental and simulated spectra (4000 K)*

(c) Imaging interferometry

The phase shift induced by neutral gas density variations can be easily visualized using a Michelson interferometer with a CCD camera at wavelength 633 nm. The beam is enlarged using a telescope (see figure 11). Interferograms of figure 12 are obtained for different values of gap and discharge current.

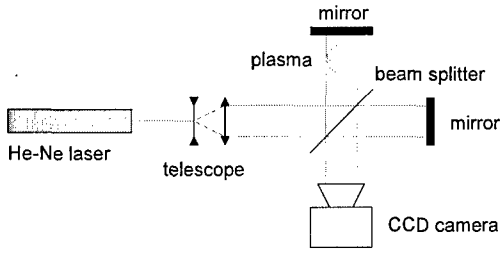

Figure 11. *Michelson interferometer*

Fringes are due to air heating around the plasma and electrodes. On the images the anode and the cathode can be distinguished. The ionized channel is an axis of symmetry for the patterns. A temperature gradient can be observed along the anode, whereas cathode is more homogeneously heated due to its greater surface, as shown by the fringes enlargement. The temperature close to the cathodic spot is higher than the temperature at the anode as expected due to the intense ion bombardment.

Figure 12. *Interference patterns for 3 mm gaps (left and center) and 1 cm (right), and 5 mA currents (left) and 25 mA (center and right)*

The observed phase shifts are in the range of several hundred radians, i.e. **several thousand degrees**. This range contrasts deeply with those of the electronic phase shifts to be measured.

II.3.B. Measurement of phase shifts at two wavelengths

(a) Procedure

For fixed discharge parameters (gap, current), the phase shift is obtained according to the following method:

- without plasma, reference (40 MHz output of signal generator), infrared and visible signals are recorded;
- idem with plasma, for different positions (values of y);
- each signal is recorded with 1 M points, on a 4 ms duration i.e. a sampling rate of 250 Me/s (25 points correspond to 4 periods, 1 M points correspond to 160 k periods);
- each signal is cut into subsignals containing a finite number of periods (actually a finite number of 4-period groups), here signals are cut into 50 subdomains having 3200 periods each;
- the spectrum of each subsignal is calculated using fast Fourier transform (FFT); at 40 MHz the FFT leads to the signal phase, plotted on a polar diagram; this gives the time evolution of the phase;
- subsignals are added to each other and averaged, and average signal/noise ratio and phase are deduced.

The acquisition of a great number a periods allows for efficient averaging and ensures coherence between averaged data, provided that the plasma remains stable during the measurement. The study of phase evolution helps to check this. Spectral analysis helps to estimate S/N and compare it to the required value (see chapter II.1).

Note that another method can be used, based on the estimation of the *scalar product* of each signal S(t), i.e. the following integrals:

$$J_1 = \frac{1}{T}\int_0^{nT} S(t)\cos(\omega t)\,dt \quad \text{and} \quad J_2 = \frac{1}{T}\int_0^{nT} S(t)\sin(\omega t)\,dt$$

$T = 2\pi/\omega$ is the 40 MHz signal period, n the number of periods in the sampled signal. If S(t) can be expressed as $S_0\cos(\omega t+\varphi)$, then $J_1 = A\cos(\varphi)$ and $J_2 = A\sin(\varphi)$. This technique leads to the signal phase and even subsignal phases. It assumes that the period is perfectly known and equal to a finite number of sampling steps, which is why devices are synchronized together.

(b) Polar diagram (measurement without plasma)

The phase evolution of the 3 measured signals, *without plasma,* is shown on figure 13.

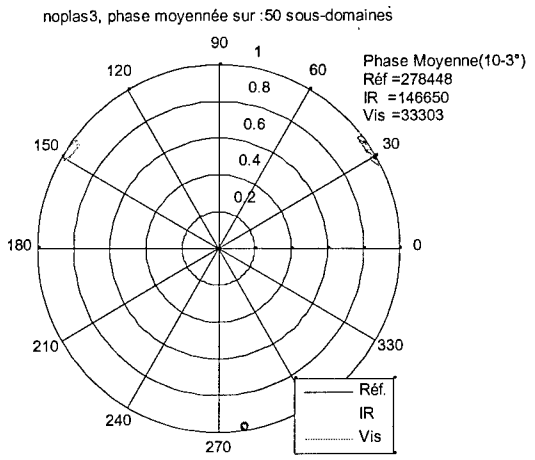

Figure 13. *Polar diagram of signal phases*

A zoom on parts of interest is shown on figure 14.

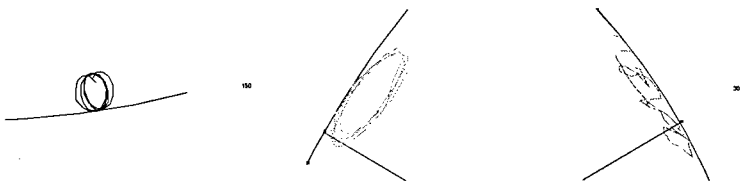

Figure 14. *Phase of reference signal (dark), infrared (red) and visible signals (blue)*

The diagrams correspond to phases deduced from subsignal spectra. In the ideal case of a perfectly constant phase, all 3 curves above would be each reduced to a single point. In reality the phase is delimited by a circle associated with the measurement error. In the present case, it can be observed that reference and infrared phases rotate around an average value whereas visible phase has a rather erratic evolution.

Rotation corresponds to amplitude modulation of the measured signals, that is directly observed as on figure 15 showing the reference signal entirely as well as its FFT spectrum.

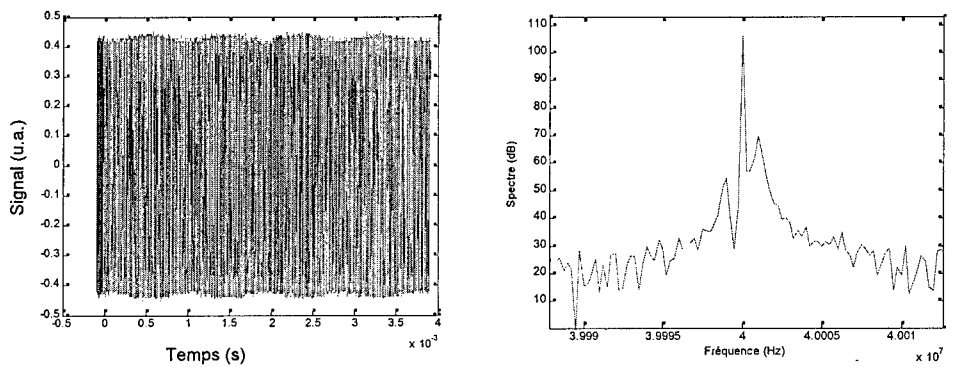

Figure 15. *(a) Reference signal and (b) its FFT spectrum*

A waveform with frequency close to 1.2 kHz is superimposed to the 40 MHz signal. It seems to be generated by the infrared AOM's 30 W power supply, due to reflexion or antenna effect or ground loop. This perturbation can be detected by plotting one point over 100 of the measured signals

(figure 16). In the ideal case of a non perturbed signal with no noise at all, the resulting graph would show a constant line. Here it shows a noisy sine waveform with 1.2 kHz frequency. This visualization technique also helps to detect synchronization problems.

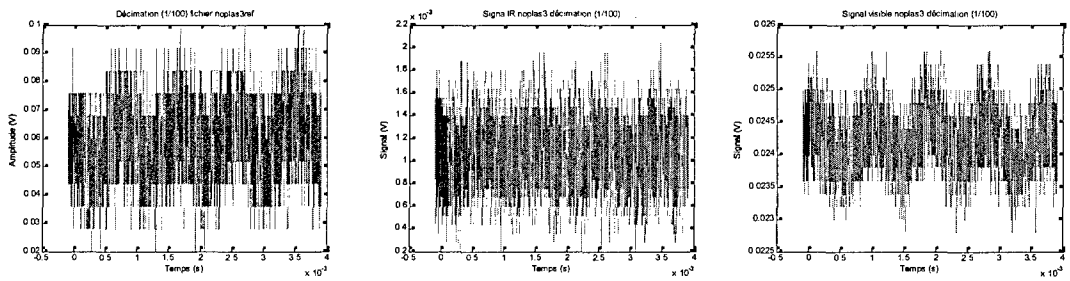

Figure 16. *Plot of 1/100 points of (a) reference, (b) infrared and (c) visible signals*

This perturbation is observed similarly on all signals. Averaging helps to overcome this problem, since the average signal exhibits regular maxima and a relatively pure 40 MHz line (figure 17).

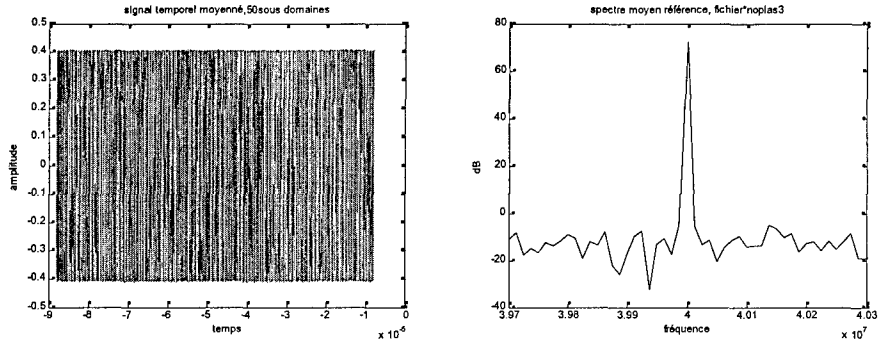

Figure 17. *(a) Average reference signal ; (b) corresponding average spectrum*

In certain cases the phase rotation center drifts during the measurement as shown on figure 18. The slope on the 1/100 point plot is a result of this phenomenon. It is observed on the reference signal showing that it is independent from any optical effect.

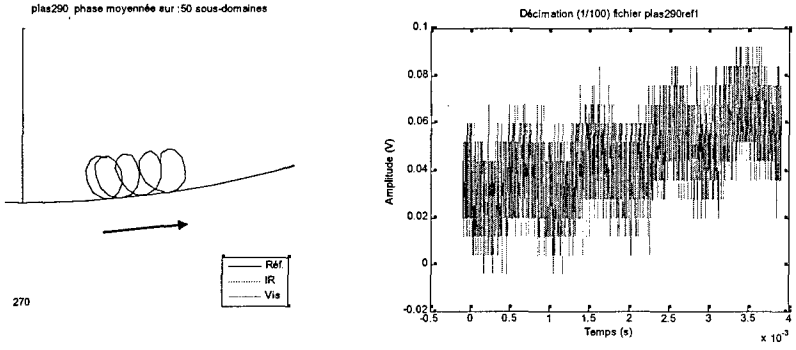

Figure 18. *(a) Reference signal phase ; (b) 1/100 point plot*

A positive phase variation corresponds to an amplitude variation of the same sign. This shows that in this particular case the acquisition time is not adapted to the measurement, and the estimated average is then less accurate.

(c) Signal/noise ratios (without plasma)

Average spectra of the three simultaneously measured signals, *without* plasma, are shown on figure 19. The measurement bandwidth (frequencies < 44 MHz) is shown here.

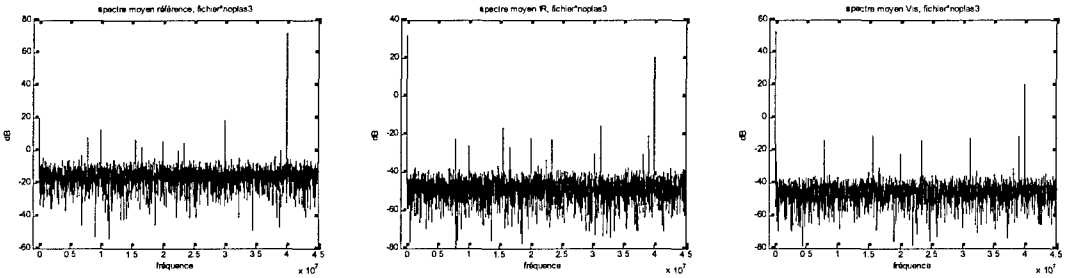

Figure 19. *Average spectra of (a) reference, (b) infrared and (c) visible signals*

All spectra show a 40 MHz line, a DC line (0 Hz) and spurious lines due to signal digitizing. Signal/noise ratios at 0 and 40 MHz are:

- reference signal: 80 dB at 40 MHz, 30 dB at 0 Hz
- infrared signal: 65 dB at 40 MHz, 95 dB at 0 Hz
- visible signal: 60 dB at 40 MHz, 95 dB at 0 Hz.

According to table 1a, the minimum signal/noise value that is sought is close to 110 dB. 30 more dB are required on the reference signal, and 45 to 50 dB on optically carried signals. In the present case noise is mainly generated by digitizing. As an illustration, lowpass filter cutoffs do not appear on the spectra. On the ohter hand spurious lines appear at higher frequencies (> 44 MHz, see figure 20a). These lines cannot come from a physical phenomenon and appear because of signal quantization after digitizing. Step-by-step jumps on the visible signal illustrate this effect (figure 20b).

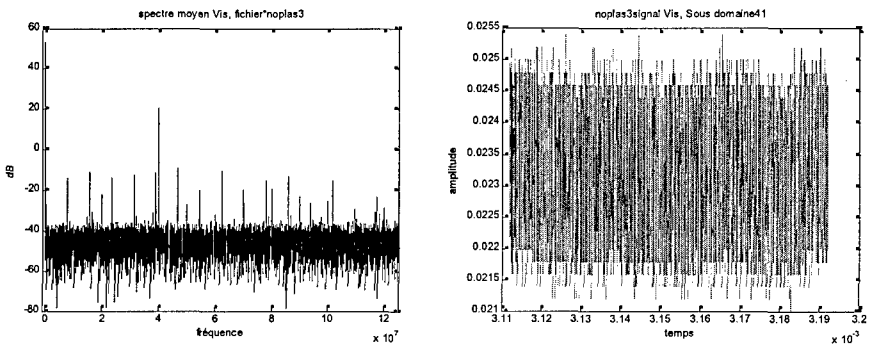

Figure 20. *Visible signal: (a) average spectrum up to 125 MHz; (b) subsignal*

To increase S/N by decreasing quantization noise, it is interesting to increase the encoding dynamic range (number of bits). An increase of 1 bit corresponds to a 6 dB gain on S/N. For reference signal, 5 more bits are thus necessary, leading to a 13 bits encoding range. Unfortunately no such oscilloscope is able to do this, and very few acquizition cards are proposed with both a high encoding range and a high sampling rate.

The optical signals require 50 more dB, so 8 to 9 more bits, which makes it unconcievable to find corresponding acquisition devices. However these signals can be improved prior to digitizing. Infrared signals have a very low magnitude (about 1 mV) and therefore close to the detection limit of the oscilloscope (minimum 2 mV per division). Visible signals have a relatively high DC component (about 20 mV) compared to the 40 MHz sine signal (about 4 mV). These signals are not

observed on full scale and then not spread on the whole encoding range. They are not actually encoded on 8 bits.
DC component can be eliminated by highpass filtering, and magnitude can be increased using a preamplifier after highpass filter. Noise factor of the amplifier must be examined in order to determine the most adequate for this purpose.

To summarize, signal quality can be improved by:
- higher encoding range to reduce quantization noise (1 bit ≡ 6 dB);
- signal amplification (also called preamplification), preceded by highpasse filtering to suppress DC components and extend the signal on the maximum scale;
- bandpass filtering to reduce spectrum folding, and increase the sampling rate for the same purpose, keeping a sufficiently high number of samples to proceed to averaging that helps to get rid of unwanted signals with a frequency that is not a mutliple of 40 MHz.

These solutions are adapted to the present detection system. Instead of an oscilloscope, a phase detector and lock-in amplifier can also be used.
In this section the phase has been examined, but not the phase shift, equal to the difference between optical phases and reference phase.

(d) Phase and phase shift drifts
Phase shift thermal drifts (without plasma)
In the present experiment the CO_2 laser has been turned on just before signal acquisition in order to limitate the risk associated with laser operation (NB: discharge in laser tube has been maintained but the shutter inside the cavity was opened just during the measurement). As a fact, signal hardcopying required a few minutes due to the great number of points (one file for one signal is about 30 Mbytes).
During the measurement, it has been observed that the *average* phase shift, particularly the visible phase shift, tends to drift with CO_2 laser exposure time of the interferometer. The following graph shows the average phase shift evolution measured after several exposure times (figure 21).

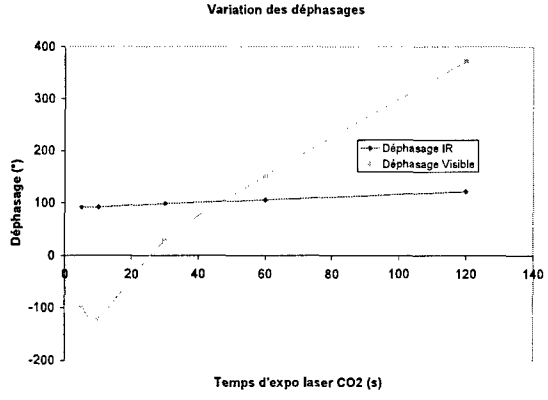

Figure 21. *Average phase shift evolution with CO_2 laser exposure time*

The infrared phase shift varies of about 30°, whereas the visible phase shift varies of 460°. The ratio of phase shift variations is consistent with the wavelength ratio, according to the following relation between phase shifts without plasma:

$$\frac{\Delta\varphi_1}{\Delta\varphi_2} = \frac{\lambda_2}{\lambda_1}$$

In the present case phase shift ratio is close to 16, compared to the wavelength ratio which is equal

to 10.6/0.633 = 16.7.
Such a drift is possibly due to the optical length variation between both branches of the interferometer, and most likely because of optical elements heating due to laser fluence.
The laser fluence is therefore probably too high for this experiment, and should be reduced to a value lower than 1 W.

Mechanical drift of visible phase (without plasma)
Figure 14c has shown an erratic variation of the visible signal phase. This variation appears even without CO_2 laser beam as shown on figure 22a. The 1/100 point plot (figure 22b) shows magnitude variations superimposed to the 1.2 kHz perturbation that can modify the phase. However these variations are relatively low and cannot explain phase variations in the range of 30°. The most probable cause of such variations is the propagation of vibrations to optical elements. The interferometer has been covered to limitate natural convection effects that can possibly perturb the measurement. On the other hand the optical table is mounted on penumatic legs so that external vibrations are dampened. Therefore vibrations are generated on the table, and 3 possible sources can be listed: CO_2 laser's water cooling system which has an uncontrolled flow rate (public water); infrared AOM which has the same cooling system, and in general, both AOMs in which an acoustic wave is generated. The infrared AOM is screwed to its mounting system, whereas the visible AOM is just glued using nail polish.

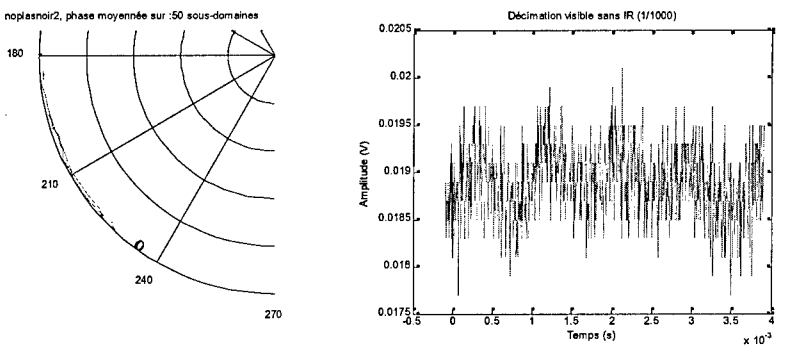

Figure 22. *Measurements without CO_2 laser beam: (a) visible phase, (b) 1/100 point plot*

(e) Phase shift measured with plasma
Infrared and visible phase shifts have finally been measured across the plasma for different values of y (coordinate orthogonal to the laser beam). The average infrared phase shift is plotted vs. y on figure 23. The position is directly read on the micrometer with which the plasma is moved (smallest scale: 10 μm).

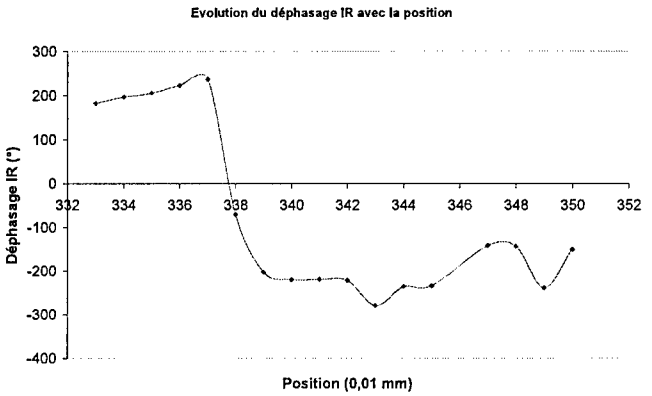

Figure 23. *Infrared phase shift vs. position in the plasma*

This phase shift is perturbed by all the causes listed above, and particularly the thermal drift. The observed evolution corresponds mainly to the neutral gas index variation, that is rather unstable and hardly reproducible.
The visible phase shift is not plotted here, because of the high uncertainty on it, due to the decrease of the interference signal detected on the photodiode. Figure 24 shows the average signal levels and average S/N ratios at both wavelengths vs. position in the plasma.

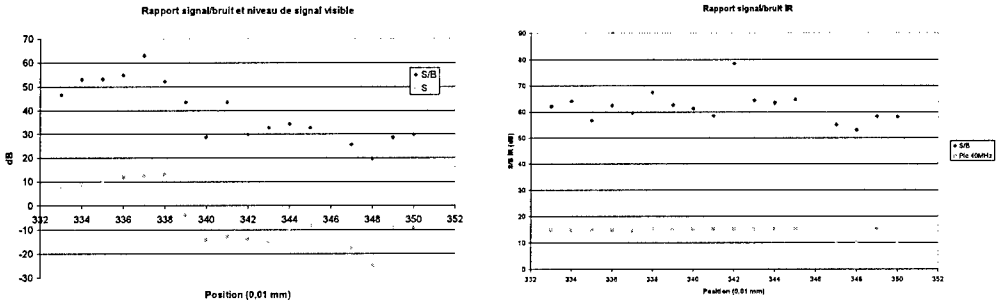

Figure 24. *Average signal levels and S/N ratios (a) visible, (b) infrarouge*

It can be noticed that the average visible signal level drops after a certain position, leading to a decrease of S/N of almost 30 dB. In the infrared the signal level remains constant on most of the observed range, except at the highest positions corresponding to zones closer to the inner plasma channel.

The most probable explanation for this is test beam refraction, the hot plasma and surrounding air acting like a diverging lens, and then misalignment of test and reference beams and finally total or partial disappearance of the interference area on the detector. Beams are most sensitive to refraction in the visible range due to air dispersion relation:

$$n(\lambda)=1+A+\frac{B}{\lambda^2}$$

$A = 2.9\times10^{-4}$, $B = 1.6\times10^{-18}$ m^2. The λ^{-2} term has been neglected in the phase shift calculation in the considered range of wavelengths. However it might have an influence on beam refraction because of its integration on the hot zone path and then would justify why the visible beam is more sensitive to refraction than the infrared one.

The impact on phase estimation is particularly strong, since subsignal phases become totally erratic as shown on polar diagrams of figure 25, corresponding to positions 341 and 348 in the plasma. The visible phase is almost impossible to determine at position 348.

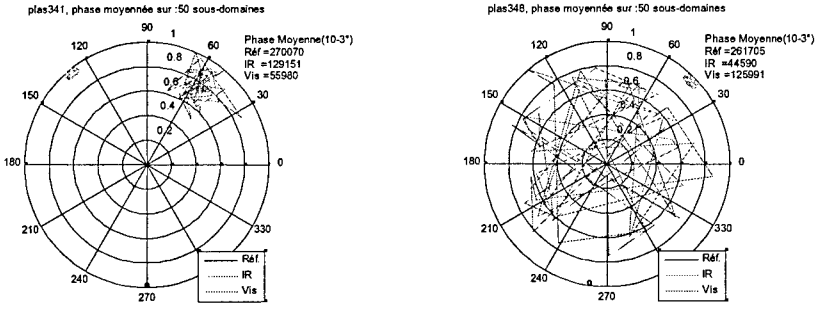

Figure 25. *Polar diagrams at positions y = 3.41 and y = 3.48 mm*

The spectrum of a subsignal shows this phenomenon, since the 40 MHz line is almost entirely drowned into bruit (figure 26).

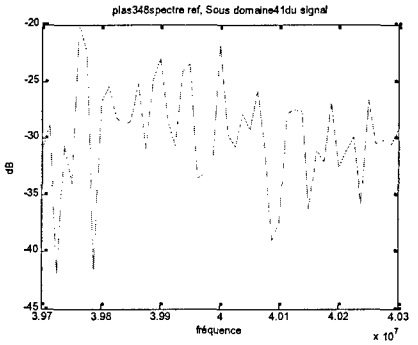

Figure 26. *Spectrum of a visible subsignal at position y = 3.48 mm*

This problem can be overcome by reducing the distance between plasma and detector, or using higher wavelengths. In the case of a higher diameter plasma sources at 100 μm and 10 μm could be employed.

Part III

Summary - Conclusions

III.1. Theoretical possibility of the measurement

The tests presented in this report do not reject the possibility of measuring phase shifts as low as 10^{-3} degrees. It is however necessary to proceed to some modifications in the detection and acquisition system in order to reach such a precision.
One point that has not been considered above is the relative alignment of visible and infrared beams that cross the plasma. A relatively low beam shift compared to the other beam can induce a relatively large error on the measured phase shift compared to the value to measure (see Annex). This does not reject the principle of the measurement, but also puts the choice of wavelengths into perspective.

III.2. Experimental proof of $N_e(r)$ measurement

The spatially resolved N_e measurement has not been proved by the present tests. However many possible problems have been identified and solutions have been proposed. The experiments that have been performed give an insight for a future experiment.

III.3. Other possible methods for N_e measurement

With heterodyne interferometry, it can be considered to modulate the current in the plasma. Leipold et al [10] have measured the density in a DC discharge by periodically pulsing the discharge and progressively increasing the duty cycle to tend to a DC regime. It could be possible to modulate the current without turning off the plasma, with a period smaller that the characteristic time of neutral gas temparature variation.
Instead of interferometry Thomson scattering can be used. The measurement remains uneasy but in principle allows for the detection of relatively low densities down to 10^{-10} cm^{-3}.
Note that Stark broadening has not been considered here since no data is available for the species present in air plasmas, and unless impurities are introduced (hydrogen, rare gases), this method is impossible to apply to air plasmas.

References

[1] R.H. Stark, K.H. Schoenbach, « Direct current glow discharges in atmospheric pressure air », Appl. Phys. Lett. 74 p.3770 (1999)
[2] Abdel-Aleam Hefney Mohamed, « Scaling and characterization of direct current glow discharge plasma in atmospheric pressure air », Ph-D thesis dissertation, Old Dominion University (2004)
[3] F. Adler, E. Kindel, « Absolute determination of electron density in a micro hollow cathode discharge by dual wavelength interferometry », Proc. 26th Int. Conf. on Physics of Ionized Gases (ICPIG), Greifswald 15-20 July 2003, 1 p.157
[4] D.R. Baker, S.T. Lee, « Dual laser interferometer for plasma density measurements on large tokamaks », Rev. Sci. Instrum. 49 p.919 (1978)
[5] C.W. Gowers, C. Lamb, « A vibration compensated high frequency heterodyne CO_2 laser interferometer for plasma diagnostics », J. Phys. E: Sci. Instrum. 15 p.343 (1982)
[6] G. Braithwaite *et al.*, « JET polari-interferometer », Rev. Sci. Instrum. 60 p.2825 (1989)
[7] P. Acedo *et al.*, « CO_2 and He-Ne two-color laser interferometry for low and medium electron density measurement on the TJ-II Stellerator », Rev. Sci. Instrum. 75 p.4671 (2004)
[8] W.A. Gambling, H. Edels, « The high-pressure glow discharge in air », Brit. J. Appl. Phys. 5 p.36 (1954)
[9] D. Staack, B. Farouk, A. Gutsol, A. Fridman, « Characterization of a dc atmospheric pressure normal glow discharge », Plasma Sources Sci. Technol. 14 p.700 (2005)
[10] F. Leipold, R.H. Stark, A. El-Habachi, K.H. Schoenbach, « Electron density measurements in an atmospheric pressure air plasma by means of infrared heterodyne interferometry », J. Phys. D: Appl. Phys. 33 p.2268 (2000)

Annex : estimation of phase variation with position

We consider here $\Delta N(r) = N(r)-N_a$ where N(r) is the air density radial distribution close to the plasma and N_a the ambient air density ($p = 10^5$ Pa, T = 293 K). A parabolic gas density profile is assumed:

$$\Delta N(r)=\Delta N_c\left(1-\frac{r^2}{R^2}\right)$$

The associated phase shift of a beam propagating along x is:

$$\Delta\varphi(y)=\frac{2\pi A}{\lambda N_0}\int_{-X}^{+X}\Delta N_c(x,y)\,dx$$

with N_0 the air density under normal conditions ($p = 10^5$ Pa, T = 273 K), $X = (R^2-y^2)^{1/2}$ and $x^2+y^2 = r^2$. With the above distribution it leads to:

$$\Delta\varphi(y)=\frac{8\pi A\Delta N_c}{3\lambda N_0}\sqrt{R^2-y^2}\left(1-\frac{y^2}{R^2}\right)$$

The variation of the phase shift with a variation of y is sought here. The partial derivate of $\Delta\varphi$ with the y parameter is:

$$\frac{\partial\Delta\varphi}{\partial y}=-\frac{16\pi A\Delta N_c}{3\lambda N_0}y\left(\frac{1-y^2/R^2}{\sqrt{R^2-y^2}}+\frac{\sqrt{R^2-y^2}}{R^2}\right)$$

The total radius corresponds to the zone where air is heated around the plasma channel. Typically it is about a few centimeters long. The range of interest of y for the measurement of electron density is lower than 1 mm. Therefore it can be assumed that $y << R$, which lets us simplify the previous expression:

$$\frac{\partial\Delta\varphi}{\partial y}=-\frac{32\pi A\Delta N_c}{3\lambda N_0}\frac{y}{R}$$

Finally the variation is expressed like:

$$\delta(\Delta\varphi)=\frac{\partial\Delta\varphi}{\partial y}\delta y$$

With a radius R = 4 cm and a central temperature $T_c = 4000$ K, the variation of y that corresponds to a -10^{-3}° phase shift (about -10^{-5} rad) is estimated for a wavelength of 633 nm.
It leads to $\delta(\Delta\varphi) = -3.32\times10^5\, y\, \delta y$.

For y = 5 µm: δy = 6 µm
For y = 50 µm: δy = 0,6 µm
For y = 500 µm: δy = 60 nm

The error on the phase shift, if the measurement is made with a 10% precision, is 10^{-4} rad. At the wavelength 10.6 µm, a similar measurement would lead to a phase shift that is 16.7 times lower, so close to 10^{-5} rad. According to table 1a, it is the value of phase shift that is sought with CO_2 laser. In order to make this measurement possible it is necessary to align the beams with a precision of a few microns across the plasma.

ONERA

Frank Reidy Research Center for Bioelectrics

Frank Batten College Of Engineering & Technology
Applied Research Center

Old Dominion UNIVERSITY

Electron density mapping of atmospheric pressure glow discharge in air using two-wavelength interferometry

Jérôme PONS, Weidong ZHU, Nobuhiko TAKANO, Karl H. SCHOENBACH
Frank Reidy Research Center for Bioelectrics, Old Dominion University, Norfolk, VA

Alexey BUGAYEV
Applied Research Center, Old Dominion University, Newport News, VA

PURPOSE : measuring electron densities with spatial resolution in the range $10^{13\text{-}15}$ cm^{-3} in atmospheric pressure air glow discharges
METHOD : 2-wavelength (10.6 and 0.633 μm) heterodyne (40 MHz) interferometry [1]
APPLICATION : electromagnetic wave absorption in the Radar range

(1) DISCHARGE SETUP AND PROPERTIES

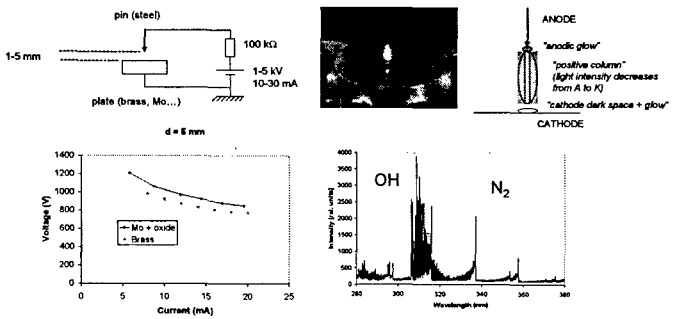

(2) INTERFEROMETER : Mach-Zehnder configuration

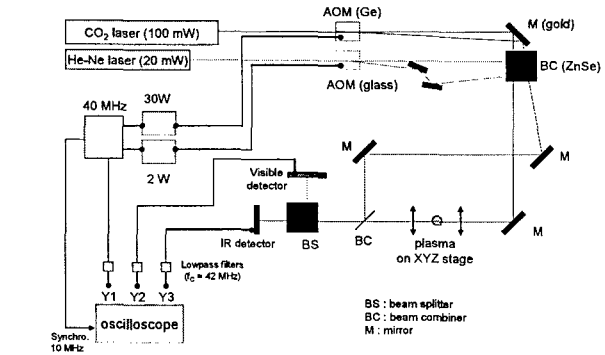

$$\int_L N_e(x)dx = -[\lambda_1\Delta\varphi_1 - \lambda_2\Delta\varphi_2]/[r_e(\lambda_1^2 - \lambda_2^2)]$$

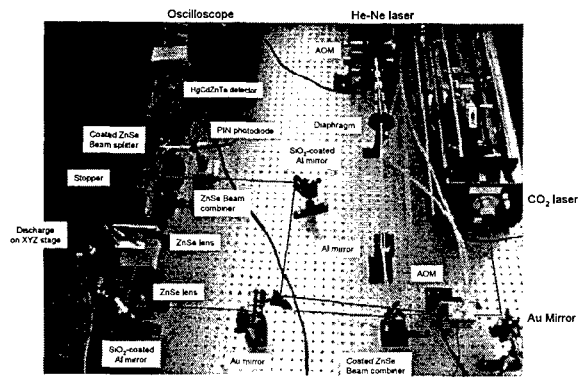

N_e (cm^{-3})	10^{12}	10^{13}	10^{14}	10^{15}
$\Delta\varphi_e$ (degrees)	$1.6 \cdot 10^{-4}$	0.0016	0.016	0.16

(3) HETERODYNE DETECTION

Principle

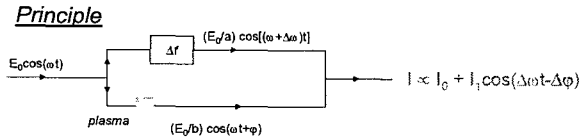

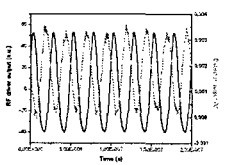

→ *post-processing*

Reference signal φ_R
IR signal φ_1
Visible signal φ_2

$$\Delta\varphi_1 = (\varphi_1 - \varphi_R)_{plasma} - (\varphi_1 - \varphi_R)_{no\ plasma}$$
$$\Delta\varphi_2 = (\varphi_2 - \varphi_R)_{plasma} - (\varphi_2 - \varphi_R)_{no\ plasma}$$

$$\int_0^{nT}\cos(\omega t+\Delta\varphi)\times\cos(\omega t)dt \propto \cos\Delta\varphi$$
$$\int_0^{nT}\cos(\omega t+\Delta\varphi)\times\sin(\omega t)dt \propto \sin\Delta\varphi \Rightarrow \Delta\varphi = \arctan(\sin\Delta\varphi/\cos\Delta\varphi)$$

Requirements :
- signal/noise > 90 dB (0.002 deg. precision)
- large number of periods for cos and sin determination
- stability during the recording time

Noise power $P = \beta f_{BW}/N$ → filtering (to reduce bandwidth) and large recording lengths
β spectral density. f_{BW} bandwidth, N recording length (# points)

Filters : low-pass, Chebyshev (f_c = 42 MHz)
Recording length : 1MS w. 250 MS/s (recording time 4 ms), Tektronix TDS7404

(4) PRESENT STATUS AND FUTURE DEVELOPMENTS

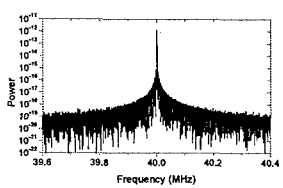

FFT infrared signal :
S/B ≈ 70 dB

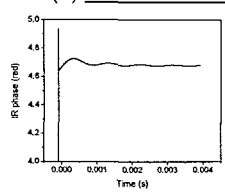

Phase evolution with time
→ *Instabilities are observed* during data recording and between two recordings

Future developments:
- Improved filtering → *bandpass instead of lowpass*
- Improved signal stability → *RF perturbation reduction, vibration / convection reduction*
- Direct phase detection → *lock-in amplification*

ACKNOWLEDGEMENTS
This work has been supported by the Radar and Electromagnetism Dept. at ONERA (French Research Institute on Aeronautics) and the Air Force Office of Scientific Research.

[1] F. Adler, E. Kindel, Proc. 26th ICPIG, 15-20 July 2003 (Greifswald) vol.1 p.157